



OPEN

Preparation of sisal fiber/polyaniline/bio-surfactant rhamnolipid-layered double hydroxide nanocomposite for water decolorization: kinetic, equilibrium, and thermodynamic studies

Mehrdad Negarestani^{1✉}, Soheil Tavassoli², Saba Reisi³, Negar Beigi¹, Afsaneh Mollahosseini^{2✉}, Majid Hosseinzadeh¹ & Asiyeh Kheradmand¹

Sisal fiber is a potent economical biomaterial for designing composites because of its low density, high specific strength, no toxic effects, and renewability. The present study utilized sisal fiber as a starting material and subjected it to modification to produce a sisal fiber/polyaniline/bio-surfactant rhamnolipid-layered double hydroxide nanocomposite material denoted as SF@PANI@LDH@RL. The composite was evaluated for its efficacy in removing reactive orange 16 (RO16) and methylene blue (MB) from aqueous solutions. The synthesized adsorbent was characterized by FTIR, XRD, and SEM-EDS techniques; these analyses indicated the successful modification of the sisal fiber. The primary factors, including contact time, adsorbent dosage, dye concentration, temperature, and pH, were optimized for achieving the most excellent adsorption efficiency. On the one hand, methylene blue removal is enhanced in the basic solution (pH = 10). On the other hand, reactive orange 16 adsorption was favored in the acidic solution (pH = 3). The highest adsorption capacities for methylene blue and reactive orange 16 were 24.813 and 23.981 mg/g at 318 K, respectively. The Temkin isotherm model, which proves the adsorption procedure of methylene blue and reactive orange 16 could be regarded as a chemisorption procedure, supplies the most suitable explanation for the adsorption of methylene blue ($R^2 = 0.983$) and reactive orange 16 ($R^2 = 0.996$). Furthermore, Elovich is the best-fitting kinetic model for both dyes ($R^2 = 0.986$ for MB and $R^2 = 0.987$ for RO16). The recommended SF@PANI@LDH@RL adsorbent was reused six consecutive times and showed stable adsorption performance. The results demonstrate that SF@PANI@LDH@RL is a perfect adsorbent for eliminating cationic and anionic organic dyes from aqueous media.

Due to the dismissal of contaminants into different habitats, eliminating industrial pollutants, such as plastic, refineries, petroleum, printing, textile, and leather, has become one of the most significant universal problems^{1–6}. In general, dyes are one of the most harmful materials in industrial effluents. The utilization of dyes has been found to cause significant and irreversible damage to the environment, posing a serious threat to both marine species and humans. This is primarily due to the slow decomposition and inherent toxicity of these substances. Based on the functional groups, textile dyes are categorized. Functional groups such as indigo, sulfur, nitro, nitroso,

¹Department of Civil and Environmental Engineering, Iran University of Science and Technology (IUST), Narmak, Tehran, Iran. ²Research Laboratory of Spectroscopy & Micro and Nano Extraction, Department of Chemistry, Iran University of Science and Technology (IUST), Narmak, Tehran, Iran. ³Department of Environmental Engineering, Graduate Faculty of Environment, University of Tehran, Tehran, Iran. ✉email: Mnegarestani71@yahoo.com; Mehrdad_negarestani@alumni.iust.ac.ir; amollahosseini@iust.ac.ir

anthraquinone, and azo. Textile dyes are toxic, resistant, bioaccumulative, non-biodegradable, and carcinogenic and cause damaging consequences on the surroundings, even at low concentrations^{7–12}. Classifying dyes based on the remaining particle charge after dissolution in an aqueous solution is standard. Such classifications consist of cationic (all basic dyes) and anionic (acidic, direct, and reactive dyes), and non-ionic (dispersed dyes)^{13,14}. Reactive Orange 16, a xenobiotic monoazo dye and highly water-soluble recalcitrant (pka = 3.75), is basically dangerous and has carcinogenic and mutagenic impacts on people. Methylene blue (Methylthionium chloride), a subset of the thiazine family, is a non-biodegradable, water-soluble cationic dye with a pka of 3.8. Therefore, the removal of dyes from the effluent is assumed to be an environmental issue^{14–17}. Numerous methodologies have been employed for the elimination of synthetic dyes from polluted water. These include techniques such as extraction, membrane separation, adsorption, photocatalytic degradation, biological treatment, oxidation, filtration, flocculation, and coagulation^{18–22}. Owing to being uneconomical, complex, and time-consuming, some of these standard techniques have been limited²³. Discovering the most coherent and straightforward dye wastewater treatment approach is crucial. Adsorption is the best choice due to its clarity and flexibility in design and insensitivity to toxic contaminants in recent decades²⁴. The quality of the adsorbent plays a crucial role in adsorption efficiency. Various types of sorbents, such as zeolite, silica, clay, chitosan, biochar, synthetic adsorbents (e.g. waste rubber tires, active carbon, mesoporous carbon substances, polymers, and filter membranes), have been studied for their effectiveness in removing pollutants from wastewater^{25,26}. The layered double hydroxide (LDH), also known as the hydrotalcite-like layered structure, is a highly effective adsorbent that enables adjustable usage densities and enhances chemical homogeneity to a significant extent. The diversity of structural compositions, morphologies, and multiple synthetic strategies make LDHs readily engineered for specific adsorption processes with enhanced performance. The anionic interaction ability of LDH is significantly influenced by its design, which involves the incorporation of divalent and trivalent metal ions within the layers. This design is dependent on synthetic requirements and the intended application of the LDH²⁷. The general formula for layered double hydroxide is shown as $[M_{1-x}^{2+}M_x^{3+}(OH)_2]^{x+}[A^{n-}]_{x/n} \cdot zH_2O$, where M^{2+} and M^{3+} are divalent cation (such as Co^{2+} , Ni^{2+} , Cu^{2+} , Zn^{2+} , Ca^{2+} , Mg^{2+}), and trivalent cation (such as Ga^{3+} , Al^{3+} , Fe^{3+} , Cr^{3+}), respectively. The typical anions representing the interlayer of layered double hydroxides are chloride, nitrate, hydroxide, carbonate, sulfate, and larger anion similar to polyoxometalates²⁸. Because the anion with the negative charge assists in maintaining the brucite-like sheets with positive charge via electrostatic attractions, the entire charge of LDHs is positive. Different parts of these layered materials, such as low price and simple synthesis, high surface area, ion exchange ability, and swelling capabilities, make them a proper choice for a dye adsorbent²⁹. Rhamnolipids (RL) are a category of anionic glycolipid biosurfactants created by different bacteria, such as *Pseudomonas aeruginosa*. The aforementioned substitutes for synthetic chemical surfactants in cosmetics and medicines exhibit potential due to their eco-friendliness and minimal toxicity. The molecular structure of rhamnolipids consists of 3-(3-hydroxyalkanoyloxy) alkanooate, wherein hydrophobic acyl chains are linked to a hydrophilic component comprising no more than two rhamnose molecules. An enhanced evaluation of biosurfactant utilization, particularly rhamnolipid-based ones, can be advantageous for the textile dye industry^{30,31}. So far, only a limited number of studies have explored the effect of modified cellulosic fiber materials coupled with LDHs on emerging pollutant elimination. For instance, a polypyrrole/polyaniline modified composite based on sisal was synthesized for capturing dyes from water. The maximum adsorption capacity of 12.43 mg/g was reported for reactive orange 5³². In another study, cellulosic sisal fiber supported with conducting polymers was developed for the adsorption of ibuprofen from synthetic wastewater, with a maximum adsorption capacity of 21.33 mg/g³³. So far, no study has been identified evaluating the synergic effects of rhamnolipid, LDH, and polyaniline as modifiers on sisal fiber for the removal of RO16 dye and methylene blue.

For the first time in this study, a potent platform was designed using SF@PANI@LDH to evaluate the removal efficiency of methylene blue and Reactive Orange 16 from effluent wastewater. The proposed adsorbent was characterized using FTIR, XRD, and SEM-EDS techniques. Different kinetic and isotherm models were employed to explain the adsorption process.

Experimental

Chemicals and equipment. Sisal fibers utilized in this study were purchased from a city bazaar in Tehran, Iran. Rhamnolipid ($\geq 90\%$) and metal salts, including nickel nitrate ($Ni(NO_3)_2 \cdot 0.6H_2O$), and aluminum nitrate ($Al(NO_3)_3 \cdot 0.9H_2O$) were provided from sigma and Aldrich. All other chemicals like Aniline ($\geq 99.5\%$), ammonium peroxydisulfate (APS), and urea were supplied from Merck, Germany, without any remediation. Hydrochloric acid and methanol were supplied from Merck (Germany) with 99% purity. Methylene blue ($C_{16}H_{18}ClN_3Na_3S$, 319.86 g/mol), and reactive orange 16 ($C_{20}H_{17}N_3Na_2O_{11}S_3$, 617.32 g/mol) were purchased from Tamadkala Company (Iran). Deionized (DI) water was used in all the experimentations.

Instruments and measurements. Modified sisal fiber morphology was examined using field emission scanning electron microscopy (SEM/EDS, Iran). The chemical structure of the modified sisal fiber was analyzed by Fourier transform infrared spectroscopy (FTIR) (Thermo AVATAR IR spectrophotometer) in the spectral range of 4000–400 cm^{-1} . Powder X-ray diffraction (XRD) was exploited to analyze the physical quality of the materials. A UV-vis spectrophotometer measured the concentrations of MB and RO16 during adsorption analyses.

Synthesis of SF@PANI@LDH@RL composite. Distilled water and methanol were used to clean the sisal fibers thoroughly, and then the fibers were dried in the oven at 328 K. The polyaniline-modified sisal fiber (SF@PANI) was fabricated in 3 steps. Initially, the cleaned sisal fibers were added into the methanol aniline solu-

tion (v/v, 20:80) and soaked for 2 h. After that, the sisal fibers were removed from the methanol aniline solution and added to the HCL solution (0.175 M), which contained 8.75 g/L^{-1} ammonium persulfate. Subsequently, it was stirred moderately at ambient temperature and pressure for 2 h. Finally, the sisal fibers were washed with water entirely and dried at 328 K.

0.610 g of $\text{Al}(\text{NO}_3)_3 \cdot 0.9\text{H}_2\text{O}$ and 0.928 g of $\text{Ni}(\text{NO}_3)_2 \cdot 0.6\text{H}_2\text{O}$ dissolved in 80 ml water aided by ultrasound for the modification of NiAl-LDH. 0.672 g of the urea and SF@PANI were eventually added to the mixture. This combination reacted at 348 K for 18 h, occurring in the atmosphere condition to acquire binary PANI and NiAl-LDHs composites modified sisal fibers (SF@PANI@LDH). After that, the prepared SF@PANI@LDH was washed entirely and dried at 328 K. As a control experimentation, this urea hydrolysis method modified LDH on the surface of sisal fiber (SF@LDH) directly. A rhamnolipid mixture is made by adding 4 g of rhamnolipid to 50 ml of warm deionized water and stirring gently for 30 min until observing a milky color. Then SF@PANI@LDH was soaked in the rhamnolipid mixture at ambient temperature and pressure for 30 h. At last, the SF@PANI@LDH was washed thoroughly and dried at room temperature. All of the mentioned stages are illustrated in Fig. 1.

Results and discussion

Characterization. Figure 2 displays the FTIR spectra of raw sisal and SF@PANI@LDH@RL. The new bands set at 2928 and 2856 result from C–H stretching vibration appearance. The peaks at 2905 cm^{-1} and 2840 cm^{-1} indicate the C–H stretching vibration of aliphatic hydrocarbons from cotton³⁴. Also, the peaks at 1720 cm^{-1} and 1665 cm^{-1} demonstrate the C–O stretching vibration of acetyl groups of lignin and hemicellulose. The peak at 1230 cm^{-1} shows second lignin. Moreover, the new peak at 1739 cm^{-1} expresses the stretching vibrations of C=O groups of rhamnolipid that demonstrates the successful modification. Surface OH of Ni/Al LDH layers and coordinated water stretching vibrations were visible at 3500 cm^{-1} in every component broadband spectra. The peaks observed at 800 cm^{-1} are indicative of the stretching vibrations associated with the metal and oxygen (M–O) bonds present in the samples. The observation of interlayer NO_3^- anions in the LDH was recorded at a wavenumber of 1385 cm^{-15} .

SEM images of the as-prepared biosorbent are provided in Fig. 3. According to Fig. 3a,b displaying the SEM pictures of plain sisal, which resembles a cylindrical bar with cracks and gaps. It is evident that there is slight porosity on its exterior surface. Figure 3c,d displays sisal after the polyaniline modification. A visual examination of these microstructures indicated that a few spherical particle colonies are created, supplying more porosity and areas valuable in pollutant adsorption. Figure 3e depicts sisal after the transformation with the LDH crystals, a delicate coating of LDH crystals with uniform size and condition developed on the sisal fiber, indicating the successful immobilization of LDHs onto the sisal fiber. The crystals were spread on the surface, delivering adequate

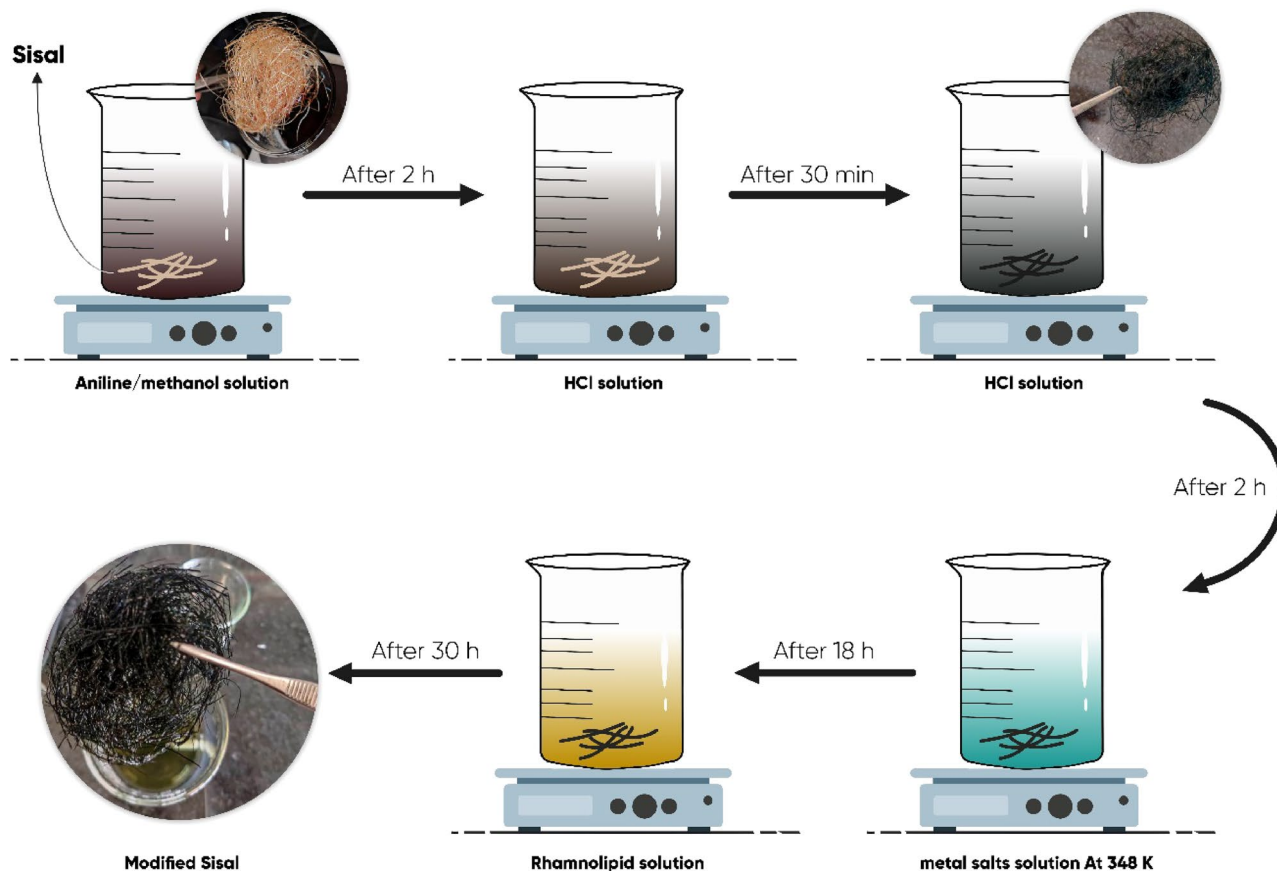


Figure 1. The synthesis procedure of SF@PANI@LDH@RL.

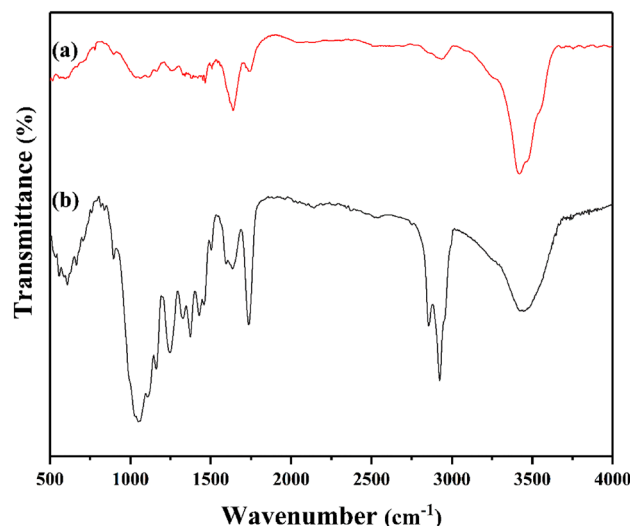


Figure 2. FTIR spectra of raw sisal fiber (a), and SF@PANI@LDH@RL (b).

functional zones for adsorption. As depicted, before the modification of LDH with rhamnolipid, NiAl-LDH has a thin (lamellar) form and stays in this structure in the company of rhamnolipid. Due to the rhamnolipid shown in Fig. 3f, these layered double hydroxide adsorbents became aggregated. These SEM pictures verify that the synthesized sisal biosorbent might be reassuring for MB and RO16 removal^{35–38}.

As shown in Fig. 4, energy-dispersive X-ray analysis was used to analyze the raw sisal fiber and the SF@PANI@LDH@RL element configurations to verify the successful modification. The sample was covered with a thin layer of gold to prevent charging of the surface and deliver a homogeneous surface for examination and imaging. The graph shows the elements of Ni and Al on the surface of SF@PANI@LDH@RL adsorbent. Carbon groups were increased in SF@PANI@LDH@RL after adding rhamnolipid to the adsorbent.

Figure 5 shows that the X-ray powder diffraction technique was used to illustrate the finalized samplings of raw sisal and SF@PANI@LDH@RL. The patterns of all materials match the simulated pattern. The graph displays intense peaks at $2\theta = 15.2^\circ$, and 23.9° attributed to the existence of cellulose in sisal fiber. Moreover, peaks at $2\theta = 11.2^\circ$, 35.1° and 39.4° confirmed the successful LDH formation. Employing rhamnolipid will enhance the interlayer distance of the end nanocomposite. According to Fig. 5, XRD patterns confirm that the space between the layers of SF@LDH@RL was more than that of one of the Ni/Al-LDH. This contrast is because of the rhamnolipid anion inside the layers^{39–41}.

Comparison of sisal and SF@PANI@LDH@RL. Sisal is an economical biosorbent that is a potent fit for dye elimination. Like other natural fabrics, sisal possesses a negative surface that can draw positive varieties with electrostatic attraction assistance. Nonetheless, adsorption will not happen due to repulsive powers when the intended combination has a negative surface. A novel SF@PANI@LDH@RL biosorbent was designed to solve this significant issue. The removal efficiency of RO16 and MB by sisal and SF@PANI@LDH@RL are compared in Fig. 6a and b, respectively. The outcomes demonstrated that the efficiency of SF@PANI@LDH@RL for RO16 was 6.25 and for MB was 5 times greater than raw sisal. Thus, the synthesized SF@PANI@LDH@RL was a potent adsorbent for dye removal.

The effect of operational factors. *Effect of contact time.* The influence of contact time enhances the equilibrium adsorption of pollutants between dyes and modified sisal, offering the promising potential for removing MB and RO16. The removal efficiency of RO16 and MB are illustrated in Fig. 7a,b SF@PANI@LDH@RL adsorption capacity for MB and RO16 ranges from 0 to 200 min. According to Fig. 7a,b MB and RO16 uptakes had average speeds and reached equilibrium at 100 min. During this period, more than 90% of MB and RO16 were eliminated from solutions; then, from 100 to 200 min, the adsorption capacity peaked in both graphs. Multiple active areas are initially available for MB and RO16, so the adsorption rate is high before it reaches equilibrium. After reaching the point of equilibrium, the active regions became fully saturated, resulting in the inability of further analyte molecules to be adsorbed into the substances, ultimately leading to the termination of adsorption.

Effect of adsorbent dosage. Adsorption dosage is a crucial factor in the adsorption procedure Owing to economic and industrial problems. Utilizing massive quantities of adsorbent raises additional pollution sources in the surroundings and causes a costly purification procedure Fig. 7e shows the MB and RO16 adsorption capacity and removal efficiency results at various adsorbent doses in the range of 20–100 mg. MB and RO16 removal efficiency enhanced from 48 and 20%, respectively, to almost 99% by improving the adsorbent doses from 20 to 100 mg. Accordingly, it is concluded that as the sorbent dose grows, numerous active areas for dye removal

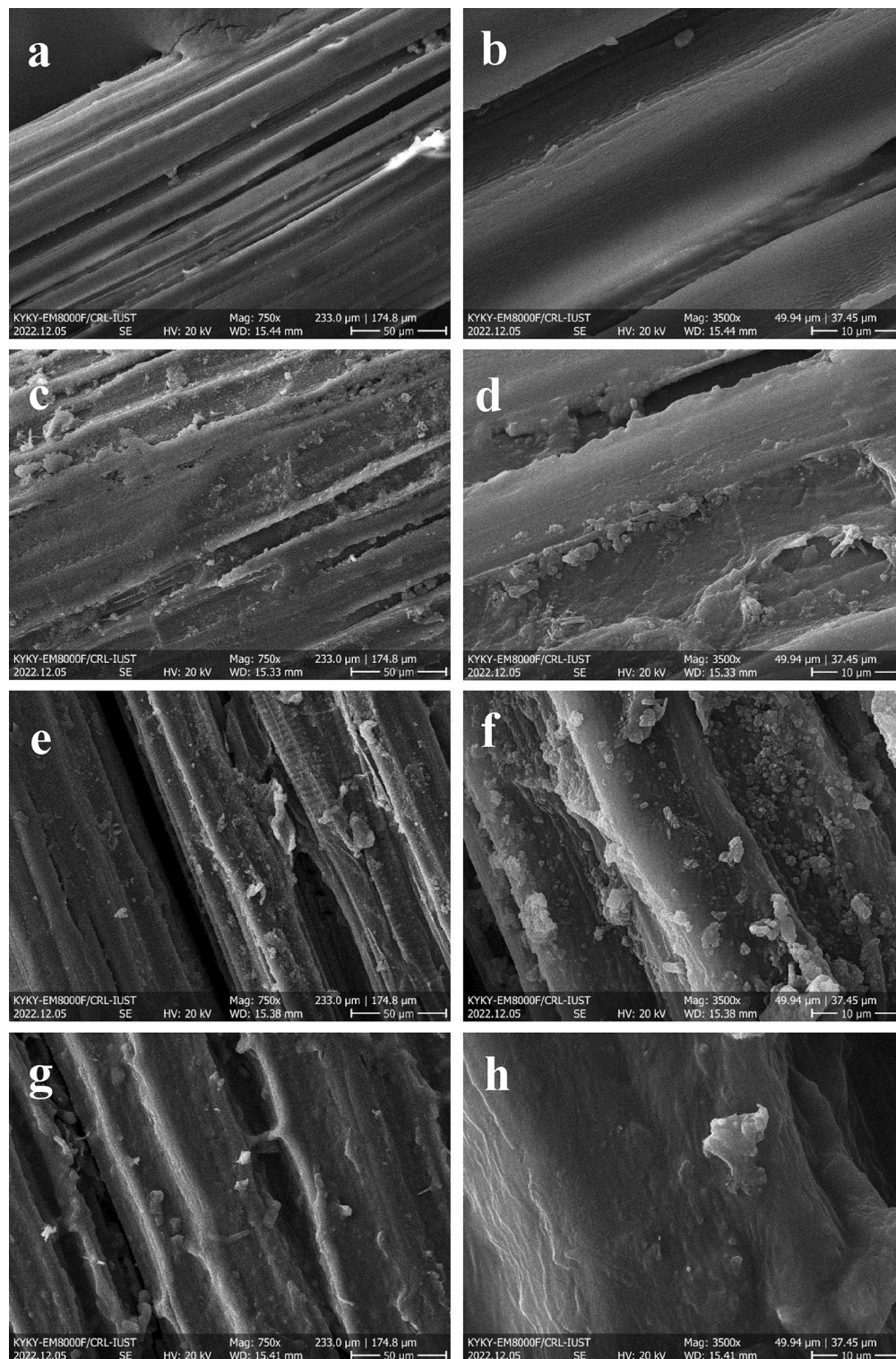


Figure 3. SEM pictures of raw sisal fiber (a,b), SF@PANI (c,d), SF@PANI@LDH (e,f) and SF@PANI@LDH@RL (g,h).

become available. A 100 mg sorbent dosage was selected in the subsequent analyses to optimize the remaining aspects because it offered the highest efficiency toward dye elimination.

Effect of dye concentration. As displayed in Fig. 7c,d the influence of starting MB and RO16 concentrations on adsorbent performance was also evaluated. The most significant removal efficiency of 99% was detected at both MB and RO16 concentrations of 40 ppm and 20 ppm, respectively. The lowest removal of 40% for MB and 50%

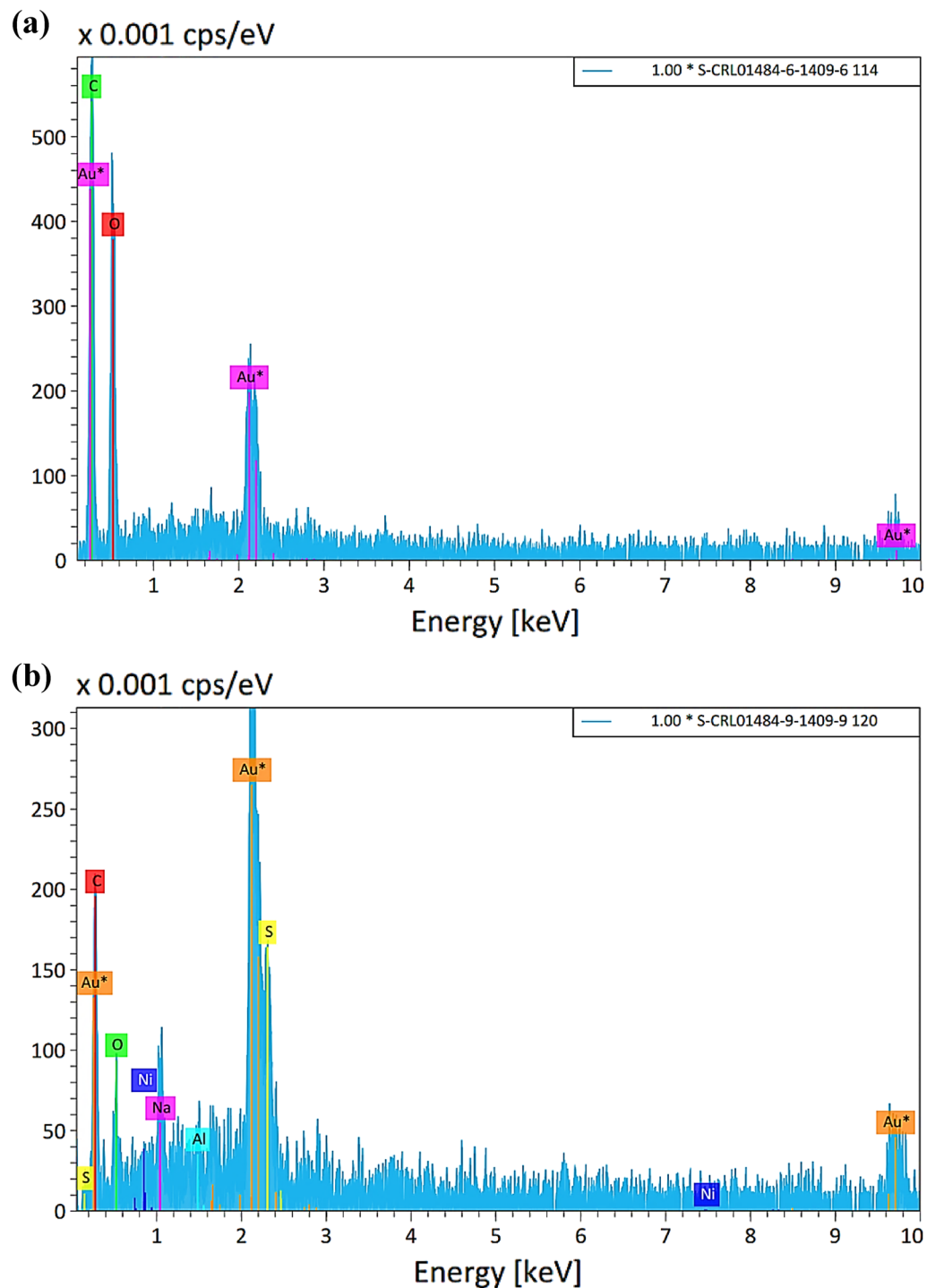


Figure 4. EDS analysis of raw sisal fiber (a), and SF@PANI@LDH@RL (b).

for RO16 was seen at 120 mg/L and 100 mg/L, respectively. Thus, all accessible active sites on modified sisal were stable, and the number of pollutant molecules grew as the concentrations of MB and RO16 grew. Higher dye concentrations will result in lower removal efficiency because these required sites have not been accessible and vacant. Nearly all of the MB and RO16 were eliminated. For further experiments, the initial dye concentrations of MB and RO16 were chosen as 40 mg/L and 20 mg/L, respectively.

Effect of temperature. The temperature optimization is shown in Fig. 7f. As observed, 313 K has the most acceptable outcome for MB and RO16 and delivers the best adsorption efficiency. It is evident that the two reactions are endothermic because the adsorption is elevated at high temperatures.

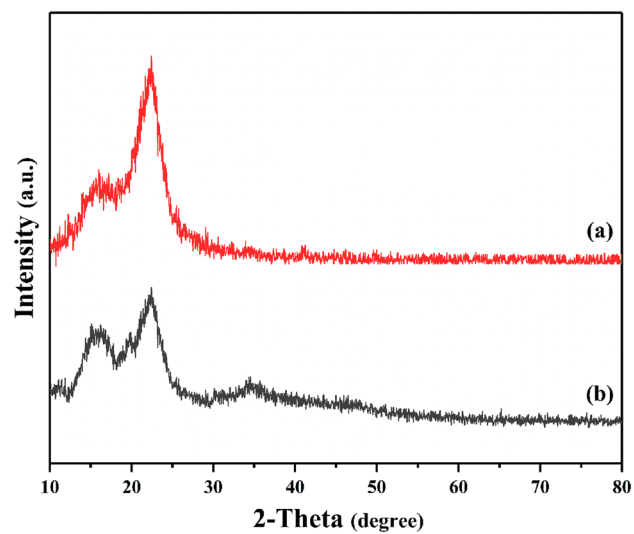


Figure 5. XRD images of raw sisal fiber (a), and SF@PANI@LDH@RL (b).

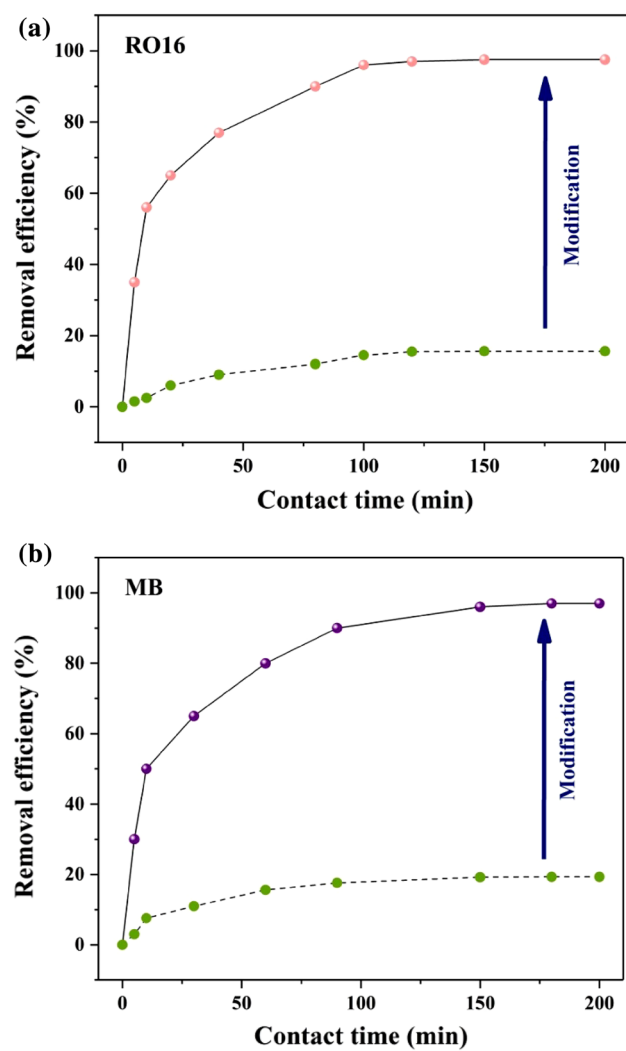


Figure 6. Comparison of SF@PANI@LDH@RL with raw sisal in terms of RO16 removal (a) and MB removal (b).

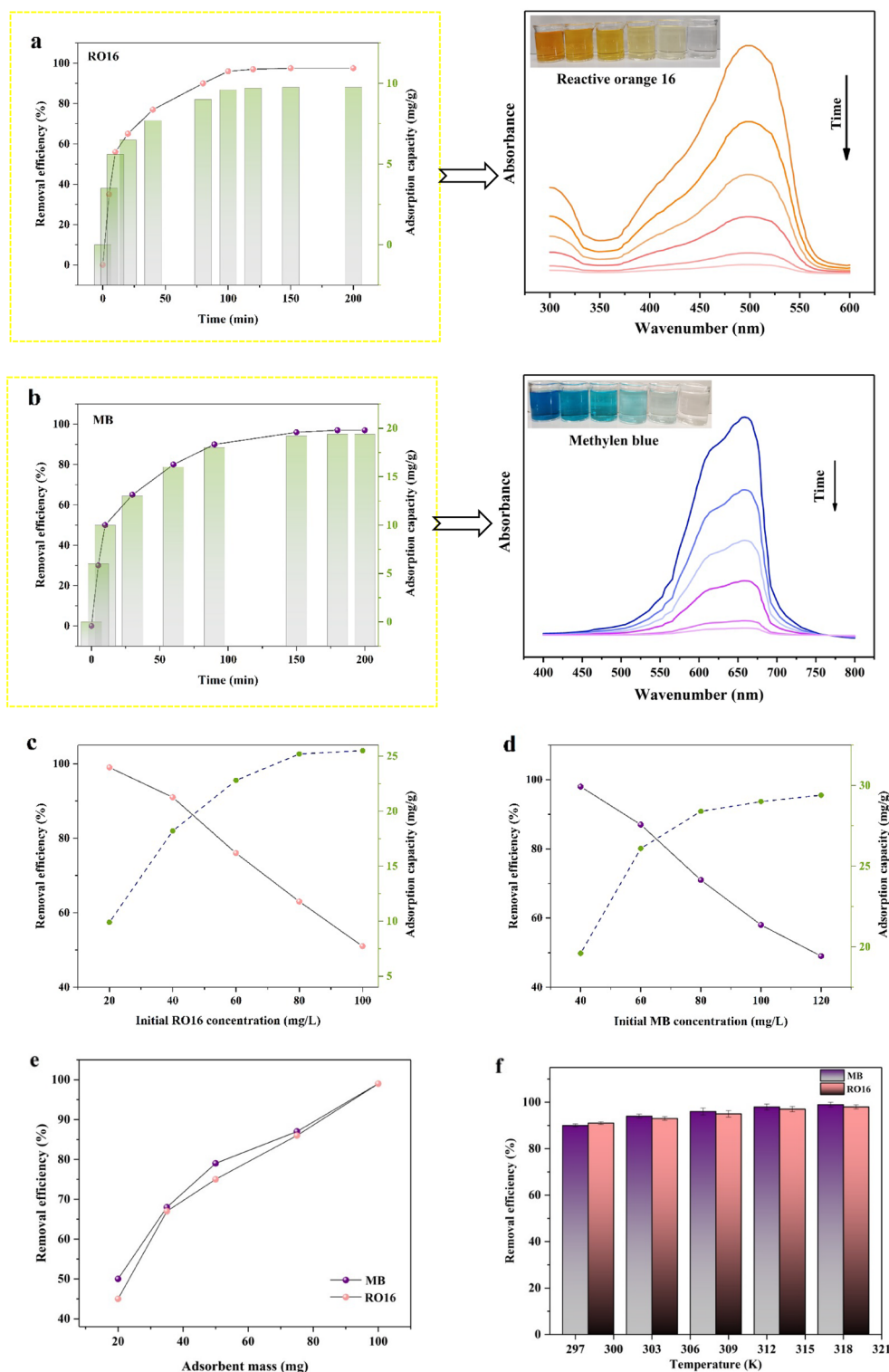


Figure 7. The effect of contact time (a,b), RO16 concentration (c), MB concentration (d), adsorbent dosage (e) and temperature (f).

Effect of pH. The surface charge of the substance and the examined dyes is extensively conditional on the pH of the solution. The pH can adjust the molecular structures of the adsorbates, the surface charge of the adsorbent, and the ionization extent. The pH of the solution plays a crucial role in determining the interaction between the adsorbent and the dyes MB and RO16, as it governs the ionization behavior of the species present in the solution⁴².

As depicted in Fig. 8, the adsorption efficacy of MB is observed to decrease upon lowering the pH to the acidic range. According to the graph, the best pH for MB elimination is 10, which will be utilized for further investigations. MB has π -conjugated electron density in its construction, but the suggested SF@PANI@LDH@RL does not possess π -conjugated electrons; consequently, it will exclude π - π stacking interaction. Simultaneously, the adsorbent may interact with positively charged MB through cation- π interaction, occurring effectively on both the upper and lower sides of the MB. Furthermore, the modified sisal can form hydrogen bonds with the nitrogen zone of the dye via its hydroxyl groups, leading to efficient adsorption. In contrast, the graph depicts a complete reversal for the RO16. The molecular structure in question lacks an extended π -conjugated arrangement. The adsorption efficiency of RO16 reached its apex by reducing pH to 2. According to the graph, the best pH for RO16 elimination is 2, which will be utilized for further investigations. RO16 ionizes into anion formation at low pH, influencing the electrostatic interaction with the adsorbent with a positive charge. Furthermore, the existence of hydroxyl groups in the RO16 molecule results in the formation of hydrogen bonds with the hydroxyl functional groups present on the proposed adsorbent.

Adsorption isotherms. Understanding the partitioning behavior of MB and RO16 molecules with the solution and SF@PANI@LDH@RL as an adsorbent is essential to design an optimum adsorption method. This article will present several commonly used adsorption isotherm equations, such as Temkin, Langmuir, and Freundlich, in order to analyze experimental data obtained from the adsorption process⁴³. First of all, the equation below demonstrates the non-linear form of the Langmuir isotherm:

$$q_e = \frac{q_m K_L C_e}{1 + K_L C_e}.$$

q_e (mg/g) shows the equilibrium adsorption capacity, and q_m (mg/g) represents the maximum adsorption capacity. K_L (L/mg) indicates the constant of the model, and C_e (mg/L) shows the equilibrium concentration of dye. The basics of Langmuir isotherm are presented as a dimensionless equilibrium parameter (R_L):

$$R_L = \frac{1}{1 + K_L C_0}.$$

C_0 (mg/L) is the maximum initial concentration of the analyte, and K_L is the Langmuir constant. R_L shows the variety of adsorption to be either favorable ($0 < R_L < 1$), unfavorable ($R_L > 1$), linear ($R_L = 1$), or irreversible ($R_L = 0$). Langmuir isotherm considers homogeneous adsorption and single-layer coverage of the modified sisal surface by dye without any interaction among analyte molecules. Hence, Freundlich isotherm was proposed as a reversible model, which is a model for surface heterogeneity and not restricted to monolayer formation to fix the mentioned problem:

$$q_e = K_f C_e^{1/n}.$$

q_e (mg/g) shows the equilibrium adsorption capacity, and C_e (mg/L) represents the equilibrium concentration of dye. K_f (mg/L) is the relative adsorption capacity, and n indicates adsorption intensity. The adsorption heat among MB and RO16 and modified sisal is defined by the Temkin model, which is presented as the following equation:

$$q_e = \left(\frac{RT}{b_T} \right) \ln(K_T C_e).$$

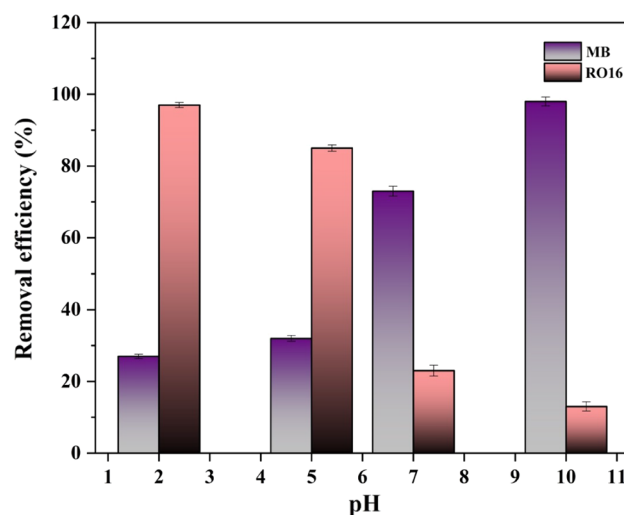


Figure 8. The effect of pH for RO16 and MB removal by SF@PANI@LDH@RL.

R represents the universal gas constant (8.314 J/mol. K), b_T (J/mol) has a relation with the adsorption heat constant, K_T shows the equilibrium binding constant (L/g), and T (K) is the temperature. The evaluation of the adsorption isotherm of RO16 and MB for modified sisal was conducted at a temperature of 298 K. The statistical analysis was performed using the Temkin, Langmuir, and Freundlich isotherms. Figure 9 depicts the relationship between the adsorption capacity and the equilibrium concentrations of MB and RO16, utilizing a non-linear methodology. In both cases of MB and RO16 elimination, the R^2 values of the Temkin isotherm are higher (0.983 for MB and 0.996 for RO16), which concurs with experimental adsorption statistics. The Temkin isotherm model deems the binding energies spread uniformly and considers the indirect reaction between the modified sisal and the dyes. The Temkin isotherm hypothesis is that the adsorption heat declines linearly when the surface coverage grows. The outcomes proved that the adsorption procedure of MB and RO16 could be regarded as a chemisorption procedure. Temkin isotherm allows measuring the heat of the adsorption; positive b_T will result in an exothermic process. Furthermore, other R^2 values are not small. Regarding MB removal, the R^2 value for the Freundlich model was 0.965 and for the Langmuir model was 0.959. Regarding RO16 removal, the R^2 value for the Freundlich model was 0.981 and for the Langmuir model was 0.914. Based on the Temkin model, the n factor makes significant values regarding the adsorption procedure. $\frac{1}{n} < 1$ according to our estimation; therefore, chemical bonds can be formed on the heterogeneous surface of modified sisal in dye elimination. Consequently, the heat adsorption of all dyes among the layers declined coverage of the adsorbent nanocomposite^{13,31}. Table 1 shows numerical studies of isotherm models.

Adsorption kinetics. Kinetic factors mostly describe the adsorption efficiency since rapid kinetics is vital in aqueous medium adsorption. Four standard kinetic models, including pseudo-first-order (PFO), pseudo-second-order (PSO), Elovich, and fractional kinetic models, were provided for the kinetic factors of modified sisal to evaluate their experimental setup. The outcomes achieved from the kinetic models and the non-linear

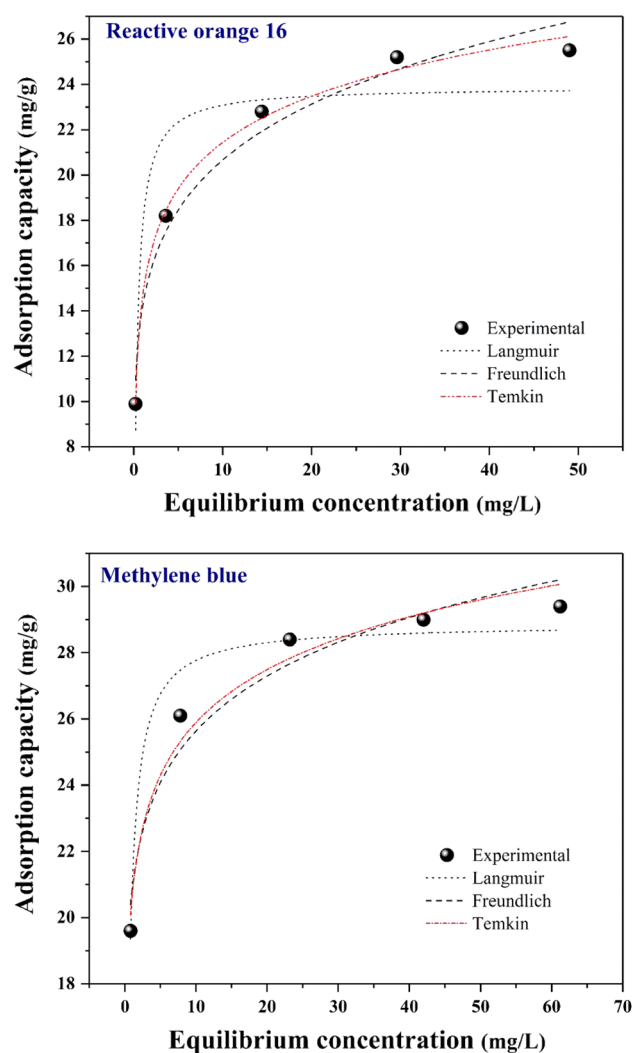


Figure 9. Isotherm fitted curves (non-linear) of RO16 and MB adsorption.

Isotherm models	Important parameters	Reactive orange 16	Methylene blue
Langmuir	$q_m(\text{mg/g})$	23.879	28.859
	$K_L(\text{L/g})$	2.89	2.545
	R^2	0.914	0.959
Freundlich	$K_F(\text{mg/L})$	14.206	20.816
	n	6.148	11.054
	R^2	0.981	0.965
Temkin	$b_T(\text{J/mol})$	883.105	1130.082
	$K_T(\text{L/mg})$	144.328	7652.461
	R^2	0.996	0.983

Table 1. Adsorption isotherm models for RO16 and MB adsorption on the SF@PANI@LDH@RL.

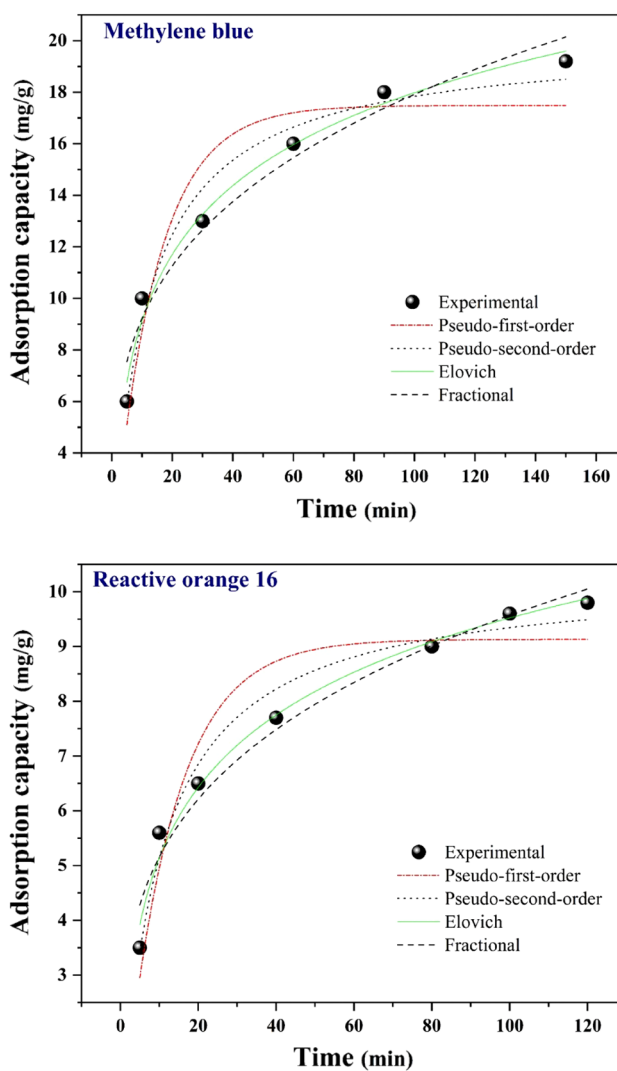


Figure 10. Kinetic plots of MB and RO16 adsorption.

curve fittings are shown in Fig. 10 and Table 2 for MB and RO16. The pseudo-first-order kinetic model is represented in the below equation:

$$q_t = q_e \left(1 - e^{-k_1 t}\right),$$

Kinetic model	Parameters	Reactive orange 16	Methylene blue
PFO	$q_e(\text{mg/g})$	9.131	17.482
	$K_1(1/\text{min})$	0.078	0.067
	R^2	0.911	0.913
PSO	$q_e(\text{mg/g})$	10.282	19.991
	$K_2(\text{g/mg min})$	0.009	0.004
	R^2	0.976	0.973
Elovich	α	2.504	3.505
	β	0.511	0.249
	R^2	0.987	0.986
Fractional	K_p	2.781	4.742
	V_p	0.268	0.288
	R^2	0.972	0.964

Table 2. Kinetic parameters pertaining to the adsorption of MB and RO16 on SF@PANI@LDH@RL.

$$\ln(q_e - q_t) = \ln q_e - k_1 t.$$

The equation below represents the PSO model, which defines the adsorption kinetics:

$$q_t = \frac{k_2 q_e^2 t}{1 + k_2 q_e t},$$

$$\frac{t}{q_t} = \frac{1}{k_2 q_e^2} + \frac{t}{q_e}.$$

k_1 (1/min) and k_2 (g/mg.min) are the rates constant of the PFO and PSO models, respectively.

Temkin adsorption isotherm equation is the root of the Elovich kinetic model. Elovich model is employed chiefly to define the chemical adsorption procedure of gas on a solid surface. The following equation represents the Elovich kinetic model:

$$q_t = \frac{1}{\beta} \ln(\alpha \beta t + 1).$$

The correlation coefficient values (R^2) were compared to determine the suitable kinetic model. As demonstrated in Table 2, (0.987, 0.986 for RO16 and MB dyes, respectively) found by Elovich were more significant than others. Accordingly, Elovich is the best-fitting model for both dyes and proves that external mass transfer and chemisorption rate could manage the dye adsorption procedures. Moreover, R^2 values obtained from Elovich for RO16 and MB were closer to one than the other models, indicating the suitability of Elovich to declare the adsorption kinetic. α represents the desorption constant (g/mg), equal to the first adsorption rate (mg/g.min), and is a constant that relates to the activation energy for chemisorption and the surface coverage. These outcomes indicate that numerous systems are involved in the adsorption of MB and RO16 by modified sisal. The equation below represents the non-linear form of the fractional power:

$$q_t = k_p t^{V_p}.$$

The antilogarithm of the intercept refers to the k_p value. q_t is the amount of adsorbed analyte at t (min). V_p is a constant typically lower than one if adsorption kinetic statistics fit into the power function model. As displayed in Table 2, R^2 values of the Fractional power kinetic model were 0.972 for RO16 and 0.964 for MB. Compared with other models, the fractional power kinetic model cannot sufficiently define the experimental statistics^{44–46}.

Adsorption thermodynamics. Table 3 displays Vant's Hoff thermodynamic parameters for MB and RO16 dyes. The equations below express the calculation of Thermodynamic parameters (ΔG° , ΔS° , ΔH°):

Dye	ΔH° (J/mol)	ΔS° (J/mol.K)	ΔG° (J/mol)				
			298 K	303 K	308 K	313 K	318 K
RO16	59,495.81	270.01	-20,968.05	-22,318.12	-23,668.18	-25,018.25	-26,368.31
MB	85,368.15	356.18	-20,773.48	-22,554.38	-24,335.28	-26,116.18	-27,897.08

Table 3. Thermodynamic parameters for MB and RO16 adsorption onto the SF@PANI@LDH@RL.

$$\Delta H^\circ - T\Delta S^\circ = -RT\ln K_D,$$

$$\Delta G^\circ = \Delta H^\circ - T\Delta S^\circ,$$

$$\Delta G^\circ = -RT\ln K_D,$$

R represents the universal gas constant [8.314 J/(mol.K)], and T refers to temperature (K). K_D indicates the distribution coefficient of the adsorption. Based on Table 3, the ΔH° values were positive in both dyes, demonstrating an endothermic approach in which more elevated temperatures lead to greater sorption for RO16 and MB over modified sisal. Typically, enthalpy values of more than 40 kJ/mol define chemisorption. In this work, enthalpy was 70.98 kJ/mol for RO16 and 84.10 kJ/mol for MB, showing a chemical adsorption procedure of dye molecular substances onto modified sisal. Table 3 shows that higher temperatures lead to more negative values of ΔG° in both RO16 and MB, and negative ΔG° values demonstrate that the adsorption process is spontaneous. So the approach was more spontaneous and possible at higher temperatures. Intercept allows understanding ΔS° (kJ/mol.K). Positive values of ΔS° in both RO16 and MB demonstrate that the system becomes more disordered. These outcomes are in sync with the experimental works of temperature impact and Temkin conclusions^{18,47}.

Adsorption mechanism. Typically, hydrogen bonds, van der Waals energies, electrostatic attraction, π - π stacking, base-acid reactions, and hydrophobic contact are the primary tools applied to water pollutants adsorption on adsorbents. In this work, substituting analytes and dyes with the interlayer anion of SF@PANI@LDH@RL is the primary cause and motivator of the adsorption approach. Different interactions simplify the adsorption occurrence. Regarding MB elimination, an interaction can occur between the π -conjugated electrons and SF@PANI@LDH@RL as a π -cation interaction with a positive charge. Because of the basic pH of the adsorption procedure, moderate deprotonation of the LDH can lead to electrostatic interaction with MB, which facilitates the adsorption. In relation to the elimination of RO16, it can be observed that the moderately protonated state of RO16 was a result of the acidic pH of adsorption. This, in turn, hindered the electrostatic attraction with SF@PANI@LDH@RL. The presence of electron density associated with π orbitals may give rise to π -cation interactions between RO16 and SF@PANI@LDH@RL. In addition, the hydroxyl (OH) functional groups have the ability to form hydrogen bonds with the hydroxides present in SF@PANI@LDH@RL. Figure 11 illustrates the removal mechanism of dyes by SF@PANI@LDH@RL.

Reusability of SF@PANI@LDH@RL. The reusability of the adsorbent has a crucial role in adsorption experiments on lab and industrial scales. This work investigated the reusability of SF@PANI@LDH@RL under optimum conditions, and Fig. 12 displays the outcomes. After washing the used sorbent with distilled water and ethanol and drying it at room temperature, SF@PANI@LDH@RL adsorbent was reused six consecutive times. Nevertheless, the adsorption efficiency was still higher than 80% for MB and RO16 even after utilizing SF@PANI@LDH@RL adsorbent six times. Thus, the outcomes indicated that SF@PANI@LDH@RL offers promising reusability in repetitious series to remove dye from aqueous solutions.

Comparison with other adsorbates. SF@PANI@LDH@RL adsorbent was compared with earlier reports in the following table, emphasizing the benefits of current results concerning adsorption capacity. All results and items are shown in Table 4. As shown, SF@PANI@LDH@RL adsorbent successfully removes MB and RO16 from aqueous solutions and has a superior adsorption capacity compared to previous reports.

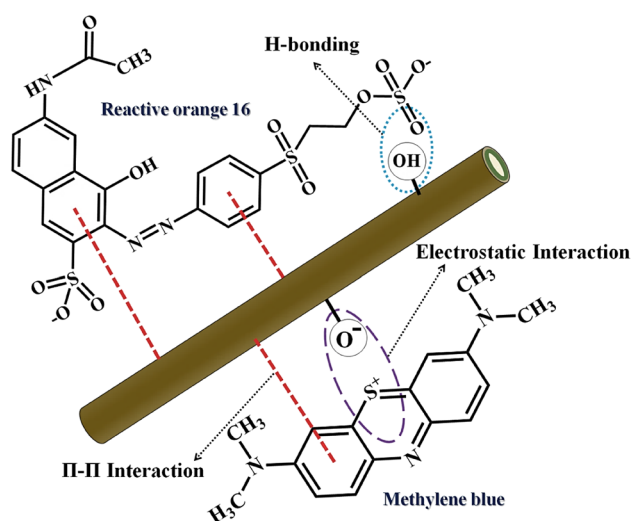


Figure 11. Dye removal mechanism by SF@PANI@LDH@RL.

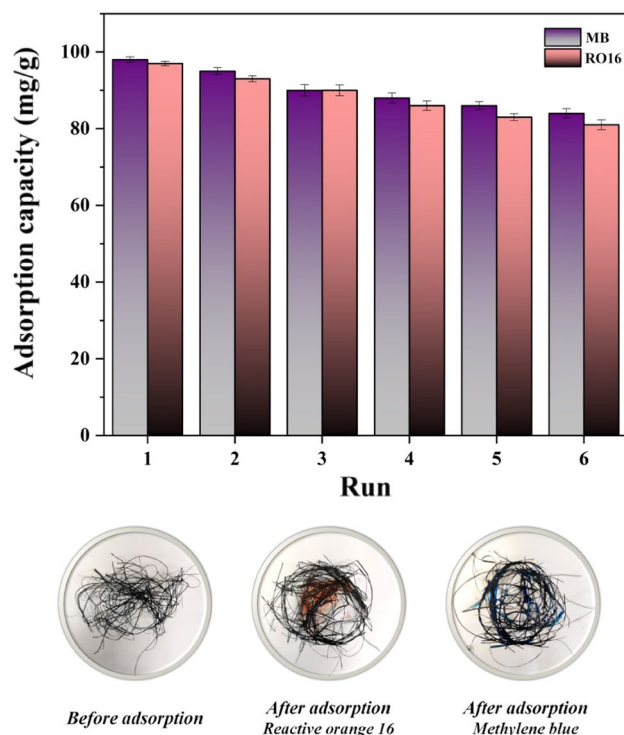


Figure 12. Reusability of SF@PANI@LDH@RL for RO16 and MB adsorption.

Adsorbent	Adsorbate	Adsorption capacity (mg/g)	Ref
Fe-BDC MOF	MB	8.65	48
Mesoporous silica nanoparticles	MB	19.26	49
g-C ₃ N ₄ loading on NiCo LDH	MB	25.16	50
CNT/eucalyptus derived activated carbon-based	MB	49.61	51
MR-Co/Al LDH	MB	54.01	52
Zeolite/activated carbon@MnO ₂ composite	MB	67.56	53
Sep-AAM	MB	99.92	54
SF@PANI@LDH@RL	MB	24.813	Present study
AC@nZVI/Ni	RO16	10.53	55
Modified zeolites	RO16	12.6	56
Activated carbon prepared from rice husk ash	RO16	13.32	57
MR-Co/Al LDH	RO16	53.04	52
Arachis hypogaea pod powder	RO16	56.48	58
m-Cs-PVA/FA	RO16	123.8	15
SF@PANI@LDH@RL	RO16	23.981	Present study

Table 4. Comparison of various adsorbents for MB and RO16 removal.

Conclusion

Eliminating organic dyes has become a global problem due to different human disorders. The adsorbent in its original state was utilized for the purpose of eliminating MB and RO16, resulting in an adsorption capacity of 24.813 and 23.981 mg/g, respectively. The optimization of the adsorption process involved the identification and manipulation of key factors such as contact time, pH, and adsorbent dosage. Moreover, the modeling analyses were conducted to gain a deeper understanding of the adsorption mechanisms. As mentioned, the Temkin isotherm was the best fit for both dye adsorption investigations showing the monolayer adsorption procedure. Moreover, the Elovich model delivered the most suitable model of the adsorption kinetics of RO16 and MB. At last, Low cost, high removal efficiency, and environmentally friendly are the distinctive benefits of SF@PANI@LDH@RL, which will supply a facile platform for dye removal from effluent wastewater. In forthcoming investigations, SF@PANI@LDH@RL could also be utilized for different impurities, including pharmaceuticals and pesticides.

Data availability

All data generated or analyzed data for the experimental part of this study are included in this published article. The data that support the findings of this study are available from the corresponding author, [Mehrdad Negarestani], upon reasonable request. Moreover, all other data that support the plots within this paper and other findings of this study are available from the corresponding author upon reasonable request.

Received: 30 May 2023; Accepted: 9 July 2023

Published online: 13 July 2023

References

- Shayesteh, H., Rahbar-Kelishami, A. & Norouzbeigi, R. Adsorption of malachite green and crystal violet cationic dyes from aqueous solution using pumice stone as a low-cost adsorbent: kinetic, equilibrium, and thermodynamic studies. *Desalin. Water Treat.* **57**, 12822–12831. <https://doi.org/10.1080/19443994.2015.1054315> (2016).
- Xiao, W. *et al.* Adsorption of organic dyes from wastewater by metal-doped porous carbon materials. *J. Clean. Prod.* **284**, 124773. <https://doi.org/10.1016/j.jclepro.2020.124773> (2021).
- Parmar, B., Bisht, K. K., Rajput, G. & Suresh, E. Recent advances in metal-organic frameworks as adsorbent materials for hazardous dye molecules. *Dalt. Trans.* **50**, 3083–3108. <https://doi.org/10.1039/d0dt03824e> (2021).
- Shi, Z., Wang, Y., Sun, S., Zhang, C. & Wang, H. Removal of methylene blue from aqueous solution using Mg-Fe, Zn-Fe, Mn-Fe layered double hydroxide. *Water Sci. Technol.* **81**, 2522–2532. <https://doi.org/10.2166/wst.2020.313> (2020).
- Eltaweil, A. S., Elgarhy, G. S., El-Subriti, G. M. & Omer, A. M. Carboxymethyl cellulose/carboxylated graphene oxide composite microbeads for efficient adsorption of cationic methylene blue dye. *Int. J. Biol. Macromol.* **154**, 307–318. <https://doi.org/10.1016/j.ijbiomac.2020.03.122> (2020).
- Nodehi, R., Shayesteh, H. & Kelishami, A. R. Enhanced adsorption of congo red using cationic surfactant functionalized zeolite particles. *Microchem. J.* **153**, 104281. <https://doi.org/10.1016/j.microc.2019.104281> (2020).
- Panda, S. K. *et al.* Magnetite nanoparticles as sorbents for dye removal: A review. *Environ. Chem. Lett.* <https://doi.org/10.1007/s10311-020-01173-9> (2021).
- Nithya, R., Thirunavukkarasu, A., Sathya, A. B. & Sivashankar, R. Magnetic materials and magnetic separation of dyes from aqueous solutions: A review. *Environ. Chem. Lett.* **19**, 1275–1294. <https://doi.org/10.1007/s10311-020-01149-9> (2021).
- Khadir, A., Negarestani, M., Pakzad, E. & Mollahosseini, A. Superior adsorption of environmental contaminants onto carbon nitride materials. In *Nanostructured Carbon Nitrides for Sustainable Energy and Environmental Applications* (eds Chowdhury, S. & Naushad, E. A.) 111–135 (Elsevier, 2022). <https://doi.org/10.1016/B978-0-12-823961-2.00006-9>.
- Khadir, A., Negarestani, M., Kheradmand, A. & Sillanpää, M. Microplastic pollution in water and their removal in various wastewater treatment plants BT. In *Microplastics Pollution in Aquatic Media: Occurrence, Detection, and Removal* (eds Sillanpää, M. *et al.*) 247–271 (Springer Singapore, 2022). https://doi.org/10.1007/978-981-16-8440-1_11.
- Khadir, A., Mollahosseini, A., Negarestani, M. & Mardy, A. Anaerobic biotechnology for the treatment of pharmaceutical compounds and hospital wastewaters BT. In *Methods for Bioremediation of Water and Wastewater Pollution* (eds Inamuddin *et al.*) 61–84 (Springer International Publishing, 2020). https://doi.org/10.1007/978-3-030-48985-4_3.
- Shayesteh, H., Raji, F. & Kelishami, A. R. Influence of the alkyl chain length of surfactant on adsorption process: A case study. *Surf. Interfaces* **22**, 100806. <https://doi.org/10.1016/j.surfin.2020.100806> (2021).
- Khadir, A., Negarestani, M., Azad, A. & Sillanpää, M. The utilization of biomaterials for water purification: Dyes, heavy metals, and pharmaceuticals. In *Novel Materials for Dye-containing Wastewater Treatment* (eds Muthu, S. S. & Khadir, A.) 27–58 (Springer, 2021).
- Negarestani, M., Etemadifar, P. & Kheradmand, A. A mini-review on the application of magnetic-based MOF for dye elimination from polluted waters. *Adv. Remov. Tech. Dye-contain. Wastewaters* https://doi.org/10.1007/978-981-16-3164-1_3 (2021).
- Malek, N. N. A., Jawad, A. H., Ismail, K., Razuan, R. & AlOthman, Z. A. Fly ash modified magnetic chitosan-polyvinyl alcohol blend for reactive orange 16 dye removal: Adsorption parametric optimization. *Int. J. Biol. Macromol.* **189**, 464–476. <https://doi.org/10.1016/j.ijbiomac.2021.08.160> (2021).
- Oladoye, P. O., Ajiboye, T. O., Omotola, E. O. & Oyewola, O. J. Methylene blue dye: Toxicity and potential technologies for elimination from (waste) water. *Results Eng.* **16**, 100678 (2022).
- Kheradmand, A., Negarestani, M., Mollahosseini, A., Shayesteh, H. & Farimaniraad, H. Low-cost treated lignocellulosic biomass waste supported with FeCl₃/Zn(NO₃)₂ for water decolorization. *Sci. Rep.* **12**, 16442. <https://doi.org/10.1038/s41598-022-20883-4> (2022).
- Motamedi, M., Mollahosseini, A. & Negarestani, M. Ultrasonic-assisted batch operation for the adsorption of rifampin and reactive orange 5 onto engineered zeolite–polypyrrole/TiO₂ nanocomposite. *Int. J. Environ. Sci. Technol.* **2022**, 1–18. <https://doi.org/10.1007/S13762-022-03951-0> (2022).
- Zhang, Y. *et al.* Application of MOFs and COFs for photocatalysis in CO₂ reduction, H₂ generation, and environmental treatment. *EnergyChem* **4**, 100078. <https://doi.org/10.1016/j.enchem.2022.100078> (2022).
- Shayesteh, H., Rahbar-Kelishami, A. & Norouzbeigi, R. Evaluation of natural and cationic surfactant modified pumice for congo red removal in batch mode: Kinetic, equilibrium, and thermodynamic studies. *J. Mol. Liq.* **221**, 1–11. <https://doi.org/10.1016/j.molliq.2016.05.053> (2016).
- Liu, X. *et al.* Metal-organic framework nanocrystals derived hollow porous materials: Synthetic strategies and emerging applications. *Innovation* **3**, 100281 (2022).
- Raji, F., Shayesteh, H. & Rahbar-Kelishami, A. YY microfluidic polymer/salt aqueous two-phase system for optimization of dye extraction: Evaluation of channel geometry. *Sep. Sci. Technol.* **57**, 2471–2481 (2022).
- Negarestani, M., Lashkari, A., Khadir, A. & Mollahosseini, A. Removal of Rifampin by Luffa: A pharmaceutical potential in producing dye in water BT. In *Novel Materials for Dye-Containing Wastewater Treatment* (eds Muthu, S. S. & Khadir, A.) 209–229 (Springer Singapore, 2021). https://doi.org/10.1007/978-981-16-2892-4_9.
- Reisi, S., Farimaniraad, H., Baghdadi, M. & Abdoli, M. A. Immobilization of polypyrrole on waste face masks using a novel in-situ-surface polymerization method: Removal of Cr(VI) from electroplating wastewater. *Environ. Technol.* <https://doi.org/10.1080/09593330.2023.2210771> (2023).
- Jawad, A. H., Malek, N. N. A., Abdulhameed, A. S. & Razuan, R. Synthesis of magnetic chitosan-fly Ash/Fe₃O₄ composite for adsorption of reactive orange 16 dye: Optimization by Box-Behnken design. *J. Polym. Environ.* **28**, 1068–1082. <https://doi.org/10.1007/s10924-020-01669-z> (2020).
- Krishna Kumar, A. S. *et al.* Heavy metal and organic dye removal via a hybrid porous hexagonal boron nitride-based magnetic aerogel. *NPJ Clean Water* **5**, 24. <https://doi.org/10.1038/s41545-022-00175-0> (2022).
- Jijoe, P. S., Yashas, S. R. & Shivaraju, H. P. Fundamentals, synthesis, characterization and environmental applications of layered double hydroxides: A review. *Environ. Chem. Lett.* **19**, 2643–2661. <https://doi.org/10.1007/s10311-021-01200-3> (2021).

28. Li, M. *et al.* Potent and durable antibacterial activity of ZnO-dotted nanohybrids hydrothermally derived from ZnAl-layered double hydroxides. *Colloids Surf. B Biointerfaces* **181**, 585–592. <https://doi.org/10.1016/j.colsurfb.2019.06.013> (2019).
29. Sriram, G. *et al.* Surface engineering of silica based materials with Ni–Fe layered double hydroxide for the efficient removal of methyl orange: Isotherms, kinetics, mechanism and high selectivity studies. *Chemosphere* **287**, 131976. <https://doi.org/10.1016/j.chemosphere.2021.131976> (2022).
30. da Silva, V. L. *et al.* Rhamnolipid from *Pseudomonas aeruginosa* can improve the removal of direct orange 2GL in textile dye industry effluents. *J. Mol. Liq.* **321**, 114753. <https://doi.org/10.1016/j.molliq.2020.114753> (2021).
31. Kheradmand, A. *et al.* Design and preparation magnetic bio-surfactant rhamnolipid-layered double hydroxide nanocomposite as an efficient and recyclable adsorbent for the removal of Rifampin from aqueous solution. *Sep. Purif. Technol.* **304**, 122362. <https://doi.org/10.1016/j.seppur.2022.122362> (2023).
32. Khadir, A., Negarestani, M. & Ghiasinejad, H. Low-cost sisal fibers/polypyrrole/polyaniline biosorbent for sequestration of reactive orange 5 from aqueous solutions. *J. Environ. Chem. Eng.* **8**, 103956. <https://doi.org/10.1016/j.jece.2020.103956> (2020).
33. Khadir, A., Motamedi, M., Negarestani, M., Sillanpää, M. & Sasaki, M. Preparation of a nano bio-composite based on cellulosic biomass and conducting polymeric nanoparticles for ibuprofen removal: Kinetics, isotherms, and energy site distribution. *Int. J. Biol. Macromol.* <https://doi.org/10.1016/j.ijbiomac.2020.06.095> (2020).
34. Kalidhasan, S. *et al.* Microwave assisted solvent free green preparation and physicochemical characterization of surfactant-anchored cellulose and its relevance toward the effective adsorption of chromium. *J. Colloid Interface Sci.* **372**, 88–98. <https://doi.org/10.1016/j.jcis.2012.01.013> (2012).
35. Li, Y., Bi, H.-Y. & Jin, Y.-S. Facile preparation of rhamnolipid-layered double hydroxide nanocomposite for simultaneous adsorption of p-cresol and copper ions from water. *Chem. Eng. J.* **308**, 78–88 (2017).
36. Li, Y., Bi, H.-Y., Liang, Y.-Q., Mao, X.-M. & Li, H. Synthesis of novel magnetic rhamnolipid-activated layered double hydroxides nanocomposite for simultaneous adsorption of Cu (II) and m-cresol from aqueous solution. *Powder Technol.* **386**, 350–360 (2021).
37. Li, Y., Mao, X.-M. & Liang, Y.-Q. Synthesis and characterization of camptothecin-rhamnolipid-layered double hydroxide nanohybrid and its controlled release property. *J. Dispers. Sci. Technol.* **41**, 1496–1503 (2020).
38. Li, Y., Bi, H.-Y., Li, H. & Jin, Y.-S. Adsorption of Cu (II) on rhamnolipid-layered double hydroxide nanocomposite. *Clays Clay Miner.* **64**, 560–570 (2016).
39. Mittal, J. Recent progress in the synthesis of layered double hydroxides and their application for the adsorptive removal of dyes: A review. *J. Environ. Manag.* **295**, 113017. <https://doi.org/10.1016/j.jenvman.2021.113017> (2021).
40. Hou, T. *et al.* Efficient removal of graphene oxide by Fe₃O₄/MgAl-layered double hydroxide and oxide from aqueous solution. *J. Mol. Liq.* **284**, 300–306. <https://doi.org/10.1016/j.molliq.2019.04.005> (2019).
41. Jung, I.-K., Jo, Y., Han, S.-C. & Yun, J.-I. Efficient removal of iodide anion from aqueous solution with recyclable core-shell magnetic Fe₃O₄@Mg/Al layered double hydroxide (LDH). *Sci. Total Environ.* **705**, 135814 (2020).
42. Dutta, S., Gupta, B., Srivastava, S. K. & Gupta, A. K. Recent advances on the removal of dyes from wastewater using various adsorbents: A critical review. *Mater. Adv.* **2**, 4497–4531. <https://doi.org/10.1039/d1ma00354b> (2021).
43. Beigi, N., Shayesteh, H., Javanshir, S. & Hosseinzadeh, M. Pyrolyzed magnetic NiO/carbon-derived nanocomposite from a hierarchical nickel-based metal-organic framework with ultrahigh adsorption capacity. *Environ. Res.* **231**, 116146. <https://doi.org/10.1016/j.envres.2023.116146> (2023).
44. Wang, H. *et al.* Kinetics and mechanism study of mercury adsorption by activated carbon in wet oxy-fuel conditions. *Energy Fuels* **33**, 1344–1353 (2019).
45. Abdel-Khalek, M. A., Abdel Rahman, M. K. & Francis, A. A. Exploring the adsorption behavior of cationic and anionic dyes on industrial waste shells of egg. *J. Environ. Chem. Eng.* **5**, 319–327. <https://doi.org/10.1016/j.jece.2016.11.043> (2017).
46. Negarestani, M. *et al.* Efficient removal of non-steroidal anti-inflammatory ibuprofen by polypyrrole-functionalized magnetic zeolite from aqueous solution: Kinetic, equilibrium, and thermodynamic studies. *Sep. Sci. Technol.* **58**, 435–453. <https://doi.org/10.1080/01496395.2022.2123743> (2023).
47. Ghosal, P. S. & Gupta, A. K. Determination of thermodynamic parameters from Langmuir isotherm constant-revisited. *J. Mol. Liq.* **225**, 137–146. <https://doi.org/10.1016/j.molliq.2016.11.058> (2017).
48. Arora, C. *et al.* Iron based metal organic framework for efficient removal of methylene blue dye from industrial waste. *J. Mol. Liq.* **284**, 343–352. <https://doi.org/10.1016/j.molliq.2019.04.012> (2019).
49. Usgodaarachchi, L., Thambiliyagodage, C., Wijesekera, R. & Bakker, M. G. Synthesis of mesoporous silica nanoparticles derived from rice husk and surface-controlled amine functionalization for efficient adsorption of methylene blue from aqueous solution. *Curr. Res. Green Sustain. Chem.* **4**, 100116. <https://doi.org/10.1016/j.crgsc.2021.100116> (2021).
50. Kaur, H., Singh, S. & Pal, B. Impact of g-C₃N₄ loading on NiCo LDH for adsorptive removal of anionic and cationic organic pollutants from aqueous solution. *Korean J. Chem. Eng.* **38**, 1248–1259. <https://doi.org/10.1007/s11814-021-0784-6> (2021).
51. Yadav, S. K., Dhakate, S. R. & Singh, B. P. Carbon nanotube incorporated eucalyptus derived activated carbon-based novel adsorbent for efficient removal of methylene blue and eosin yellow dyes. *Bioresour. Technol.* **344**, 126231 (2022).
52. Kheradmand, A. *et al.* Adsorption behavior of rhamnolipid modified magnetic Co/Al layered double hydroxide for the removal of cationic and anionic dyes. *Sci. Rep.* **12**, 14623. <https://doi.org/10.1038/s41598-022-19056-0> (2022).
53. Shojaei, M. & Esmaeili, H. Ultrasonic-assisted synthesis of zeolite/activated carbon@ MnO₂ composite as a novel adsorbent for treatment of wastewater containing methylene blue and brilliant blue. *Environ. Monit. Assess.* **194**, 1–16 (2022).
54. Kaya-Özkiper, K., Uzun, A. & Soyer-Uzun, S. A novel alkali activated magnesium silicate as an effective and mechanically strong adsorbent for methylene blue removal. *J. Hazard. Mater.* **424**, 127256 (2022).
55. Seyedi, M. S., Sohrabi, M. R., Motiee, F. & Mortazavinik, S. Synthesis and characterization of activated carbon@zerovalent iron-nickel nanoadsorbent for highly efficient removal of reactive orange 16 from aqueous sample: Experimental design, kinetic, isotherm and thermodynamic studies. *Res. Chem. Intermed.* **46**, 1645–1662. <https://doi.org/10.1007/s11164-019-04054-1> (2020).
56. Fungaro, D. A., Borrelly, S. I. & Carvalho, T. E. M. Surfactant modified zeolite from cyclone ash as adsorbent for removal of reactive orange 16 from aqueous solution. *Am. J. Environ. Prot.* **1**, 1–9 (2013).
57. Akbar Ali, A. M. *et al.* Removal of reactive orange 16 by adsorption onto activated carbon prepared from rice husk ash: Statistical modelling and adsorption kinetics. *Sep. Sci. Technol.* **55**, 26–34. <https://doi.org/10.1080/01496395.2018.1559856> (2020).
58. Chandarana, H., Subburaj, S., Kumar, P. S. & Kumar, M. A. Evaluation of phase transfer kinetics and thermodynamic equilibria of reactive orange 16 sorption onto chemically improved *Arachis hypogaea* pod powder. *Chemosphere* **276**, 130136 (2021).

Author contributions

M.N.: Experimental work, Methodology, Software, Writing—review & editing, Writing original draft. S.T.: Experimental work, Methodology, Software, Writing—review & editing, Writing original draft. S.R.: Experimental work, Methodology, Software, Writing—review & editing, Writing original draft. N.B.: Software, Writing—review & editing. A.M.: Conceptualization, Methodology, Writing—review & editing, Supervision. M.H.: Conceptualization, Methodology, Writing—review & editing, Supervision. A.K.: Software, Writing—review & editing.

Competing interests

The authors declare no competing interests.

Additional information

Correspondence and requests for materials should be addressed to M.N. or A.M.

Reprints and permissions information is available at www.nature.com/reprints.

Publisher's note Springer Nature remains neutral with regard to jurisdictional claims in published maps and institutional affiliations.



Open Access This article is licensed under a Creative Commons Attribution 4.0 International License, which permits use, sharing, adaptation, distribution and reproduction in any medium or format, as long as you give appropriate credit to the original author(s) and the source, provide a link to the Creative Commons licence, and indicate if changes were made. The images or other third party material in this article are included in the article's Creative Commons licence, unless indicated otherwise in a credit line to the material. If material is not included in the article's Creative Commons licence and your intended use is not permitted by statutory regulation or exceeds the permitted use, you will need to obtain permission directly from the copyright holder. To view a copy of this licence, visit <http://creativecommons.org/licenses/by/4.0/>.

© The Author(s) 2023